DETECTOR R & D PROPOSAL: LIQUID XENON (KRYPTON) CALORIMETRY

CERN/DRDC/90-70
DRDC/P17

J.Seguinot**, J.Tocqueville and T.Ypsilantis*.
College de France, Paris, France.

M.Bosteels, E.Chesi, A.Gougas, G.Passardi, J.Tischhauser, A.Zichichi.
CERN, Geneva, Switzerland.

R.Ferreira Marques, M.I. Lopes and A.Policarpo.
L.I.P.-Coimbra, University of Coimbra, Coimbra, Portugal.

M.Kostrikov, A.Ostankov and A.Zaitsev.
Institute for High Energy Physics, Protvino, Serpukhov, U.S.S.R.

Y.Giomataris.
World Laboratory, Lausanne, Switzerland.

Abstract: A proposal is made for R&D support to investigate*** the ultimate resolution achievable in a totally active liquid Xenon (Krypton) electromagnetic calorimeter which should lead to the construction of a 100 (400) liter prototype. Detection of either ionization or scintillation signals gives excellent energy resolution ($\sigma_E/E \leq 1\%/\sqrt{E}$) while ionization allows alone gives precise determination of the direction ($\approx$1 mr) and vertex origin ($\approx$1 mm) of a high energy photon or electron ($E \geq 25$ GeV). Large surface area photocathodes have been developed which efficiently detect the fast scintillation signal.

*spokesman
**contactman
***The data reported here were achieved within the CERN-LAA project [1]

TABLE OF CONTENTS

1. INTRODUCTION

Liquid Xenon is attractive as the sampling and showering medium of a totally active electromagnetic (em) calorimeter because it is a fast ($\tau \leq$ 20 ns) and efficient scintillator ($3 \cdot 10^4$ photons/MeV) and an efficient ionizer ($6.8 \cdot 10^4$ electrons/MeV). Drift of ionization electrons can provide highly sensitive positional information. It's relatively short radiation length of 2.8 cm allows construction of a totally absorbing $28X_0$ calorimeter in a length of 78.4 cm.

Observation of either ionization or scintillation gives an excellent measure of energy ($\approx$1%) but simultaneous observation of both can give even better resolution because the anticorrelation of these quantities allows suppression of Landau-like fluctuations, probably due to δ-rays.

Accurate position determination ($\sigma_x \approx 0.1$ mm) can be obtained by drift in short cells (d=15 mm) and directional sensitivity ($\sigma_\theta \approx 1$ mr) by depth sampling. Direction and position determinations are made without referance to the vertex origin of the photons hence these quantities may be used to determine this point, along the z axis of the collider.

It's slow drift velocity (v=3 mm/μs) presents a difficulty at high luminosity hadron colliders since the maximum drift time (t=v/d) is 5 μs. Doping with 3% methane increases v to 20 mm/μs and reduces t to 750 ns. To further increase v, studies of other dopants are planned. Even with the long integration time of 750 ns, double hits (same tower, different beam crossings) can be resolved because the fast tower scintillation signal provides an amplitude tag for the position sensitive (but slow) ionization signal.

Since cost and availability of Xenon are important factors in this project we shall evaluate the performance of a liquid Krypton calorimeter through laboratory measurements similar to those we are carrying out for Xenon. Doping of Krypton (with 1 to 5% Xenon) will probably be required to

supress the slow (85 ns) scintillation component. Krypton has the longer radiation length of 4.6 cm hence a totally active $28X_0$ calorimeter will be 128.8 cm long. This length may be acceptable in a dedicated Higgs search experiment (via photon and electron decay modes) or in forward spectrometers for B physics (see SPSC proposal P238+Add. 1, 2, 3 re B_s mixing, CP violation).

In the following text, the prototype calorimeter will be described, the work done so far will be presented and the future work outlined.

2 THE CALORIMETER CONCEPT

A tentative design of the prototype calorimeter (100 liters of liquid Xenon) is described below. It will be made with rectangular rather than trapezoidal towers to keep the volume within the available 100 liters, however an LHC design would indeed be with trapezoidal towers and pointing geometry. Resolution in energy will be obtained from the fast scintillation signal while position and direction are from depth sampled drift cells. Updates to this design will be made as new data from the test cell (described in section 3) become available.

A perspective view of the unit cell is shown in fig. 2.1a and a plane view of the tower in fig. 2.1b. The cell (and tower) have 100 μm ϕ metalized quartz wires (pitch 1 mm) strung between (&through) the 3 mm ϕ carbon fiber posts (pitch 56 mm) with 200 μm thick carbon fiber walls, floor and roof. The cell is oriented such that the axis of the electromagnetic shower is parallel to the wire array. Each cell has a depth of two radiation lengths (Δz=56 mm) and transverse size ($\Delta x=\Delta y$=30 mm). Fourteen such cells, in depth, constitute the tower and 10x10 towers make up the prototype calorimeter $(10.7X_0)^2 x (28X_0)$, as shown in fig. 2.2. Active liquid Xenon makes up ≈99% of the calorimeter mass, the remainder being carbon fiber structural material. Monte Carlo simulations (GEANT 3.14, EGS 4) of em showers show that the inactive

material of this calorimeter contributes only a small term to the energy resolution ($\sigma_E/E \approx 0.2\%/\sqrt{E}$). The Xenon (Krypton) sensitive volume will be 70 (312) liters with total volume 100 (400) liters weighing 308 (976) kg.

The tower (fig. 2.1b) has transverse walls (parallel to the wire array) which are coated with an Aluminum film and overcoated with MgF_2. These walls serve as equipotential surfaces (15 KV) and as reflecting mirrors. The floor and roof are coated with strips (80% coverage) which serve as field shaping traces as well as reflectors. A uniform electric field of 10 KV/cm, applied between the transverse walls and the earthed wire array, causes the ionization electrons to drift up to and through the Frisch decoupling grid and to be collected on the wire array. The Frisch grid, located 1.5 mm either side of the wire plane, is made of a reflecting electroformed metal mesh of 90% optical transparency. Each quartz wire (which runs the full length of the calorimeter) is metalized in 54 mm sections with 2 mm bare gaps, matching the cell pitch of 56 mm. As the wire enters a readout post, it is soldered to a resistive carbon fiber wound helically around the post. The unmetalized gap allows each of the cells (along the wire) to be readout independantly. Wave form digitizers (or flash ADC's) at each end of the resistive fiber determine the deposited charge distribution along the wire array direction (y) by charge division and along the drift direction (x) by timing. The readout therefore gives the position (x_i, y_i) of deposited charge (q_i) in the cell at depth (z_i).

A fast tower scintillation signal is detected at the end of the tower by a photosensor (Silicon or CsI diode), shown as the hatched region of fig. 2.1b. The scintillation signal and photosensor are fast ($\tau \leq 15$ ns) hence this signal can be used as part of a fast transverse energy (E_t) trigger and also to identify the beam crossing. Slow drift in the (d=15 mm=750 ns) cells can be tolerated because ionization and scintillation amplitudes are correlated hence the ionization charge (produced in the

same beam crossing as the trigger) is amplitude tagged by the large E_t scintillation trigger signal. An example of this logic is shown in fig's. 2.3. Assume that the (t=0) trigger is initiated (in part) by a 25 GeV photon which enters a particular tower (say at $\sin\theta=0.4$ hence $E_t=10$ GeV) at a position (say) 10 mm to the left of the wire array. Its ionization signal (I_1) therefore arrives at t=500 ns, as shown in fig. 2.3a. Since the shower direction is parallel to the wire plane, all its produced ionization charge arrives isochronously, especially from the early cells where the shower is still columner (see fig.'s 2.5a,b). This signal also retains the intrinsic shower width since longitudinal and transverse diffusion are small (i.e. $\sigma_l=\sigma_t=7$ ns=140 μm for 15 mm drift). A second (say t=550 ns) trigger initiated (in part) by a 50 GeV photon which hits the same tower ($E_t=20$ GeV) at a position (say) 3 mm to the right of the wires causes an ambiguity because its ionization signal (I_2) arrives at t=700 ns, before the first event is entirely collected. The scintillation signals (S_1 and S_2 in fig. 2.3b) are coincident with (and part of) the trigger and they amplitude tag the ionization signals. In real detectors, ionization and scintillation signals are not generally of equal amplitude but they are proportional hence the above argument remains valid. Of course these signals (I_1) and (I_2) sit on a background of arriving drift electrons from particles produced in earlier and later beam crossings.

A minimum ionizing hadron loses 21.4 MeV in traversing a cell and 300 MeV per tower. A fast scintillation tranverse energy threshold (E_t) of (say) 20 GeV could be triggered either by an em shower of the requisite energy (50 GeV at $\sin\theta=0.4$) or by 170 hadrons traversing the tower which seems improbable. The energy deposit due to minimum ionizing tracks coming from 1000 min. bias events (50 beam crossings both earlier and later-20 events/crossing) has been evaluated as being flat (in time) with only 21 MeV of ionization energy per 5 ns time bin. More important is the

pileup background due to minimum bias π^0's which deposit all of their energy in the calorimeter. This source is usually eliminated by the tranverse energy cut but the effect of pileup on the allowable E_t lower limit is difficult to estimate. It is evident that a Monte Carlo simulation of the π^0 and hadron pileup background must be performed to be sure of the viability of the long drift approach. Such a calculation has now been started and results may be expected at the time of the open presentation of this proposal (or before). We will submit an addendum on this subject a.s.a.p.

The left-right ambiguity is resolved by detecting an above threshold digital signal on either the left or right Frisch grid. Another independant method to resolve the left-right ambiguity will be considered later.

2.1 THE EXPECTED PERFORMANCE

A 1 GeV electron shower is shown projected onto the XZ plane of the calorimeter in fig. 2.4. An (x_i, y_i) perspective view of the z-integrated energy deposit in the first (0 to 56 mm) and second (56 to 112 mm) depth cells is shown in fig.'s 2.5a and b, respectively (from the Monte Carlo simulation program GEANT 3.14 with $\Delta x=\Delta y=0.5$ mm binning). Evidently, the energy centroid gives a precise determination of the shower position and many such determinations, in depth, gives a precise determination of the vector direction of the shower.

A spherically symmetric calorimeter was simulated with a 1 m inner radius and radial normals. Using (EGS 4) simulated data, the directional resolution σ_θ for (25, 10, 1) GeV electrons was calculated from the energy weighted centroid points (x_i, y_i) at depth (z_i) with weights $(\sigma_{xi}, \sigma_{yi})$ obtained from the width of these distributions. To remove tails only the points with more than (10, 20 or 30) % of the peak energy are used. Directional errors of σ_θ=(0.9, 1.4, 12.4) mr, respectively were found (with the 30% cuts) as shown in fig. 2.6a versus N (the number

of cells used in the fit). The projected position coordinate ρ (at the interaction point) was found with errors σ_ρ=(1.0, 1.5, 12.8) mm, respectively as shown in fig. 2.6b. The error along the beam axis $\sigma_z=\sigma_\rho/\sin\theta$ is good enough to resolve multiple interaction vertices if the photon energy $E \geq 25$ GeV and the polar angle θ is above 19^0 (i.e. $\sigma_z \leq 3$ mm for $\eta \leq 1.8$). Since the photons of interest in Higg's searches are almost always greater than 25 GeV the only limitation will be in the rapidity range. This position and direction measurement also eliminates the left-right ambiguity since only one solution intercepts the (z) beam axis. This feature of the calorimeter will reduce the H---$\gamma + \gamma$ combinatorial background by several orders of magnitude at high luminosity LHC, with 18 interactions per crossing in a length of 200 mm (i.e. ≈10 mm spacing of the vertices). Finally, the position errors σ_ρ' at the inner face of the calorimeter were found to be (50, 90, 640) μm, again for electrons of (25, 10, 1) GeV, respectively.

The energy resolution of this calorimeter will be of the form $\sigma_E/E=aE^{1/2}+b$ with $a \leq 0.5\%$ because detection of both ionization and scintillation allows supression of Landau-like fluctuations. The constant term is estimated as $b\approx(0.2\text{-}0.3)\%$ due to calorimeter leakage. The smallness of (a, b) will permit excellent resolution at both high and low energies.

It is believed that the combination of unexcelled energy and angular resolution with the asociated vertex finding capability of this device will be of decisive value for Higg's searches and other new physics at LHC. In addition, the two-gamma shower separation capability of less than 1 mm will allow excellent off-line π^0 rejection.

3. EXPERIMENTAL RESULTS

The experimental work reported here will be the subject of a more extensive report now being prepared [2].

3.1 SCINTILLATION DETECTORS

The liquid Xenon scintillation light is emitted in the wavelength interval of 175 $\pm$ 5 nm. Silicon photodiodes have been used as the photo-sensors for scintillating crystal calorimeters with a tower geometry (e.g. L3 at LEP) in which the light traverses a large fraction of the crystal length to reach the photodiode. In Xenon liquid, the distance between the shower maximum and the tower end is about 60 cm which will require excellent wall reflectivity and liquid transparency (see fig. 2.1b).

Two different in-situ photosensors have been developed and/or tested. They are a reflective CsI photocathode and a Silicon strip photodiode. The photosensor to be used in the prototype calorimeter is not yet fixed however these two solutions are shown to be viable.

3.1.1 THE CsI REFLECTIVE PHOTOCATHODE DIODE.

A CsI reflective photocathode was made by vacuum deposition onto a stainless steel substrate. The detected quantum efficiency (i.e. electrons per incident photon) was measured (with electron extraction into 1 bar methane gas) as shown in fig. 3.1 [3]. The detected efficiency at 175 nm is 0.32 which corresponds to a yield of 0.42 e per absorbed photon (CsI reflectivity =0.23).

A photosensor based on this cathode could operate by extraction of the electrons into the liquid followed by slow drift (hence small signal) to a collector grid.

An alternative photosensor (with much higher sensitivity) could be made of a 3 mm quartz entrance window followed by 1 mm of methane gas (at 1 bar) closed by the chamber body of 3 mm Boron Nitride (BN). The CsI cathode is deposited on the BN inner surface and photoelectrons are collected on metal strips (10% coverage) deposited on the inner surface of the quartz window. Such a photodiode is intrinsically fast because the electron drift time in methane is 10 ns/mm. Its capacitance per unit area

is only 88 fF/cm^2 hence a 9 cm^2 tower has a total capacitance of 0.8 pF. With this low capacitance the electronic response time will be very small ($\tau_e \leq 0.1$ ns) so that the detected pulse width is entirely determined by the Xenon scintillation lifetime ($\tau \leq 13$ ns).

The positioning of this photodiode at the end of the tower guarantees that only UV scintillation photons from the shower will be detected and the effect of the inactive materiel will be minimal. A minimum ionizing particle which traverses the 1 mm of methane gas deposits 157 eV and hence produces a direct signal of 5 e. This is extremely small compared to its scintillation signal of $9 \cdot \varepsilon_c \cdot 10^6$ e per tower (where ε_c is the photon collection efficiency). The signal ratio (direct/scintillation)$=5.6 \cdot 10^{-7}/\varepsilon_c$ is extremely small showing that hadrons which traverse the methane cannot produce a significant effect. The direct signal from the CsI is also small since the energy loss of a min. ion. particle in the 500 nm thick CsI film is 250 eV hence direct electron production in the cathode cannot be much greater (and is probably much less) than in methane. These photodiodes can be cheap compared to an equivalent area Silicon strip photodiode, but have about a factor four less detected quantum efficiency. This relative loss of quantum efficiency may be advantageous because the high CsI threshold (6.5 eV) guarantees that this cathode functions without intrinsic fluctuations i.e. the electron yield per absorbed photon is either 0 or 1 but never > 1. A related advantage of the CsI photodiode is its high absorbtivity (≈77%) compared to (27%) for a Silicon photodiode (see next section).

3.1.2 THE SILICON STRIP UV PHOTODIODE.

The quantum efficiency of a large area (18 cm^2) and high resistivity Silicon strip diode (DELPHI) was measured [4] (in collaboration with P. Weilhammer of CERN) versus photon wavelength λ, as shown in fig. 3.1. The detected quantum efficiency (i.e. electrons per incident photon) is

extremely high and is greater than 100 % in the UV region, even including reflection and absorption losses. This indicates that the yield (electrons per absorbed photon) is much greater than one and that electron collection is efficient in the strip configuration . This detector has 6 μm wide metallic strips with 25 μm pitch hence 24% opacity. At 175 nm the Silicon reflectivity is 65% so the absorbed fraction of incident photons is 0.76x 0.35=0.266 hence 1.35 detected quantum efficiency (fig. 3.1) implies a yield of 5 electrons per absorbed photon. Note that this is still within the energy limit for electron production since a 7.1 eV (=175 nm) photon can excite as many as 6 electrons into the conduction band (1.12 eV bandgap). This points out a possible problem with Silicon photosensors, namely that intrinsic yield fluctuations (Poisson?) may limit the attainable energy resolution unless an important Fano factor ($F<5\cdot10^{-4}$) limits this variance.

The capacitance of the strip detector was measured to be 20 pF/cm^2 or 230 times higher than the CsI photodiode. A strip detector covering the 9 cm^2 tower end still has only 180 pF capacitance which when coupled to a ($\Omega\approx20$ ohm) current amplifier gives the adequately fast response time of 3.6 ns. An LHC trapezoidal tower with end area of 30 cm^2 will have a capacitance of 600 pF and response time of 12 ns. This is a bit long for LHC and may require development of a lower impedance current amplifier (Ω=2 ohms) to obtain a faster electronic response.

A possible problem with the strip detectors is their extreme sensitivy to the charged particles (i.e. W_{Si}=3.6 eV/e, W_{Xe}=33 eV/photon). This should not be a problem in an em shower since the particles are absorbed early before reaching the tower end. A hadron traversal, however, can produce a direct signal of $3.3\cdot10^4$ e (in 300 μm of Silicon) as compared to its tower scintillation signal $9\cdot\varepsilon_c\cdot10^6$ e. The ratio ($0.4\%/\varepsilon_c$) is small but not negligible and requires that the photon collection efficiency be kept high (i.e. $\varepsilon_c \geq 50\%$).

3.2 THE PULSED 100KV ELECTRON ACCELERATOR.

A pulsed 100 kV electron accelerator (shown in fig. 3.2) was built and is used to inject excitation energy into the liquid. A light beam from a low pressure (200 torr) hydrogen flash lamp (FWHM=15ns) is focused onto a CsI vacuum reflective photocathode to produce the photoelectrons which are subsequently accelerated. This device can deliver as little as 1 MeV (400 electrons of 2.5 keV) or as much as 1 TeV (10^7 electrons of 100 keV) of excitation energy per pulse into the liquid, permitting the investigation of the scintillation and ionization over a wide range of total energy and specific ionization. Low energy measurements are important for high energy em calorimetry because high energy particles produce significant numbers of δ rays and because most of the shower energy is eventually degraded into excitations of Xenon via low energy electrons and photons.

The charge entering the liquid Xenon cell is monitored by a Faraday-cage collimator which intercepts about 75% of the accelerated electrons. In an independant study, the Xenon cell was replaced by a solid copper Faraday-cage disc and the transmitted charge was measured. The correlation between the intercepted and transmitted charge showed that the transmitted charge q was monitored with fractional error $\sigma_q/q \approx 0.3\%$. The transmitted energy is obviously $E=qV$ where V is the accelerator voltage, corrected for energy loss in the 12 μm thick mylar entrance window (by a GEANT3.14 simulation).

3.3. CRYOSTAT, CONDENSER AND CLEANER

A cryostat, condenser and cleaning system (fig. 3.3) was built (purposely) without high-vacuum specifications (i.e. a stainless steel vessel pumpable to high vacuum with bakeout at 300 ^{0}C) using materiels which make construction of the calorimeter practical but with enough cleaning power to remove impurities by continuous closed gas circulation. It contains Ceramics, Boron Nitride, Viton O rings, metals (all cleaned and

degassed before assembly) and a circulation pump with a neoprene diaphragm. The electron beam entrance window is made of a 12 μm thick metalized mylar foil glued over a 10 mm ϕ hole in the cell metal base. The gas which evaporates from the test cell (due to the heat load) is forced by the circulation pump through an oxisorb cartridge and molecular sieves (13X and 4A at -80 ^{0}C) and then recondensed in the heat exchanger. The pressure above the liquid is kept constant by feedback regulation of the liquid nitrogen flow in the heat exchanger, hence the temperature is constant (0.2 ^{0}C) as is the Xenon level.

To drift electrons 15 mm with 99% efficiency requires an (electron) absorption length of 1500 mm (τ=500 μs in pure Xenon) corresponding to an impurity level of 13 ppb (oxygen equivalent). An equal (photon) absorption length requires an impuriy level of only 1 ppm, hence a liquid sufficiently clean to drift electrons will allow photon transport over a distance 75 times as long. This is almost exactly the ratio needed for a calorimeter designed to drift electrons 15 mm and transport photons about 1000 mm.

Medium purity Xenon gas (Carbagas N45) was initially injected into the system and liquid was condensed. Electron drift was immediately seen and the ionization signal was monitored as a function of time (the closed points of fig. 3.4). The initial lifetime of 100 ns was very small indicating strong contamination however after 5 days of circulation through filters the lifetime increased to 4 μs. Even though the lifetime was still improving (albeit at lower rate) the run was terminated before reaching a plateau in order to try this cleaning technique with an initially purer gas.

High purity Argon gas (Carbagas N60) was, therefore, injected into the system and condensed. A long electron lifetime was immediately observed ($\tau \geq 70$ μs) without a long cleanup period. Measurements of both

ionization and scintillation (and their anticorrelation) were made, with results given in section 3.5.2.

Improved Xenon lifetime was obtained by injecting precleaned gas into the system (but with unknown contamination in transfer). The Xenon was of USSR origin and was cleaned (with high vacuum technology) to τ=160 μs by D.Schinzel and A.Gonidec of CERN. As before, the ionization signal was monitored as a function of time (the open points of fig. 3.4). The initial lifetime was higher than previously and the rate of cleanup was somehat faster. After 5 days of circulation with cleaning the electron lifetime increased to better than 100 μs, and it became difficult to measure additional improvement.

These data show that a calorimeter can be constructed of Ceramics, Boron Nitride, Viton O rings, rubber and metals without high vacuum technology. To obtain the required long lifetime it is preferable to start with a pure gas followed by continuous circulatation with purification through filters.

3.4 XENON SCINTILLATION

3.4.1 LIFETIME

First observation of the scintillation was made with a vacuum photomultiplier (PM) because it is a proven and reliable technique for photon detection. The cell (fig. 3.2) was modified, as shown in fig. 3.5, to include a re-entrant CaF_2 window and a small MgF_2 windowed PM. Upon condensing Xenon, scintillation light was immediately observed with an amplitude that confirmed the expected large yield. It showed also that the scintillation is fast and that the liquid is transparent to its own radiation.

The liquid Xenon scintillation waveform was measured as shown in fig. 3.6a. The observed width is 20 ns which (after the quadrature subtraction of the 15 ns lamp pulse width) gives an intrinsic width of 13

ns in agreement with other measurements of the Xe_2 molecule triplet state lifetime. The faster singlet state (3 ns) cannot be discerned with this long lamp pulse. It is important to note the absence of long lifetime tails. The scintillation of 1 bar Xenon gas was also measured and its waveform is shown in fig. 3.6b where a 60 ns tail is clearly visible.

3.4.2 YIELD AND LIQUID TRANSPARENCY

The scintillation yield of $3 \cdot 10^4$ photons/MeV was measured, as shown in fig. 3.7. The energy required to produce one photon is therefore 33 eV, about twice as large as the energy needed for ionization (W=15.6 eV).

To determine the liquid transparency the scintillation yield was monitored while the Xenon liquid level heigth h was varied (also shown in fig. 3.7). No significant absorption was seen in 2 cm of path length and we estimate a photon absorption length >10 cm. More work is needed to measure the real absorption length.

3.4.3 ENERGY RESOLUTION

With the set-up of fig. 3.5, a linear PM response was observed (fig. 3.8a) versus energy. The energy resolution σ_E/E was, however, limited by the photoelectron statistics $1/\sqrt{N_{pe}}$, as shown in fig. 3.8b. The small solid angle of the PM was fixed by cell geometry and PM surface area however future scintillation detectors (CsI or Silicon) will not be so limited by solid angle (photoelectron statistics). Even so, the measured resolution scaled correctly and a resolution of about 1.4% was attained at the highest energy of 20 GeV/c.

3.5 IONIZATION AND SCINTILLATION

3.5.1 XENON LIQUID

In these measurements the cell set-up was as shown in fig. 3.9 with a Silicon photodiode (glued to a ceramic backing plate) replacing the PM and a drift gap to collect the ionization electrons. The area of the Silicon

strip photodiode was (22 x 22) mm^2 and it was located 18 mm from the electron beam entrance window. Two 90% transparent electroformed metal meshes M_1 and M_2 were located 3 and 6 mm respectively from the entrance window. The mesh M_1, biased at positive potential, collected the ionization electrons through a decoupling capacitor into a low noise charge sensitive preamplifier (r.m.s. noise= σ_q =300e) while M_2 was biased to prevent any photoelectrons (possibly from the Silicon) from reaching the collector. An ionization signal was observed but the liquid was still in the early stages of purification (fig. 3.4) and the electron lifetime was only 100 ns compared to the fastest collection time of 1 μs. From this lifetime an impurity level of 65 ppm (oxygen equivalent) is inferred and correspods to a photon absorption length of 23 mm hence 55% light absorption in the 18 mm between the source and the Silicon photodiode.

Notwithstanding the light absorption and short electron lifetime, the ionization (I) and the scintillation (S) signals were measured as a function of the electric field with the results shown in fig.s 3.10a, b (for a fixed incident energy of 9 GeV/c). Note that the ionization rises whereas the scintillation decreases slightly with electric field, as expected if an anticorrelation mechanism is operative. The scatter plot (fig. 3.10c) of the I versus S shows this anticorrelation more directly. Improvement of the energy resolution will be obtained by using the specific linear combination of the signals (I+αS) which projects the points onto an axis perpindicular to this anticorrelation line. The linearity of the individual signals (I) and (S) versus incident energy are shown in fig.'s 3.11a, b. It should be emphasized that these tests to observe the anticorrelation were made before the liquid was purified, so this effect must be confirmed under better conditions (see section 3.5.2).

The energy resolutions (not shown) were reasonably good considering the short electron lifetime (in the ionization case) and a progressive

deterioration (of unknown origin) of the Silicon photodiode signal with time (in the scintillation case).

3.5.2 ARGON LIQUID

High purity Argon gas (Carbagas N60) was condensed into the cell equipped with the PM (as in fig. 3.5) but with a drift cell added (as in fig. 3.9). Both ionization (I) and scintillation (S) signals were observed versus electric field as shown in fig.'s 3.12a and b, respectively. These measurements (made with a good electron lifetime of $\tau \geq 70$ μs) show the anticorrelation mechanism is indeed operative because the ionization increases and scintillation decreases with electric field. The single charge-density model [5] predicts that the collected charge N depends on electric field E_d through the formula

$$N=N_0 \ln(1+\xi)/\xi \qquad (1)$$

as shown by the curve of fig. 3.12a with $\xi=K/v=(K/\mu)/E_d$ and N_0 the asymptotic charge. The fit parameters are $N_0=8.3\cdot10^7$e and $K/\mu=5.2$ kV/cm for a total energy E=2.25 GeV (i.e. $3.3\cdot10^4$ electrons of 66.5 keV). The W value ($=E/N_0$) is therefore 27.1 eV which may be compared to the min.ion. value of 23.6 eV. This completely normal result is in contrast to that observed in liquid Xenon (see section 3.6.1). The fit value of $K/\mu=5.2$ kV/cm, however, is higher than expected and must be further investigated.

Full anticorrelation requires $I+\alpha S=\beta$=constant. Taking the ionization signal ($I=N_0$) and as the scintillation signal ($S=N_{pe}$=the number of photoelectrons) then two measured points in fig. 3.12b fix the constants (α, β). The curve of fig. 3.12b is then simply transposed from the fit curve of fig. 3.12a. Even though it is not a fit, it represents the data quite well and indicates full anticorrelation. This confirms the original observation of this effect in liquid Argon with 1 MeV electrons by Kubota et al [6].

The energy resolution σ_E/E obtained from the ionization signal is shown in fig. 3.13. It shows the excellent resolution of $(0.3/\sqrt{E}+0.9)\%$ which characterize totally active calorimeters. Of course, in a real em shower not all the energy is deposited punctually and leakage must be added, but for sufficiently deep calorimeters ($28X_0$) this may be limited to 0.2%. The constant term (0.9%) is thought to be due to as yet uncontrolled fluctuation in the electron beam flux. In several runs, under the best conditions, a high energy resolution of 0.8% was attained.

With this PM geometry the energy resolution (from scintillation) is, as before, dominated by photoelectron statistics hence is not shown.

3.6 XENON LIQUID IONIZATION

3.6.1 CHARGE COLLECTION EFFICIENCY AND FREE ELECTRON YIELD

The cell set-up was as in fig. 3.9 except that the Silicon photodiode was removed. The electron lifetime during these measurements was excellent i.e. $\tau \geq 100$ μs. To increase the drift sensitivity, the mesh M_1 was removed and charge was collected on mesh M_2 after d=6 mm drift. The signal amplitude (mV) was measured as a function of drift time t for various electric fields E_d. The signal amplitude (mV) is converted to collected charge Q via the preamplifier sensitivity (2.5 pC/V) and fit to the formula

$$Q = Q_0(\tau/t_d)(1-\tau/t_e)^{-1}(e^{-t/te}-e^{-t/\tau}) \qquad (2)$$

where Q_0 is the asymptotic charge, $t_d=d/v$ is the maximum drift time, τ is the electron lifetime and $t_e=26.7\mu s$ is the preamplifier response time. An example of this signal is shown in fig. 3.14. The charge increases almost linearly with time with the slight curvature due to the preamplifier response time. The quantities determined by the fit are Q_0, τ and the drift time t_d. The values of $N=Q_0$ are shown in fig. 3.15 versus the electric field

E_d and fit to eq. 1. The three curves of fig. 3.15 were obtained with electron beams of (15, 37, 67) keV kinetic energy with total energies (E) of (0.64, 1.97, 4.02) GeV, respectively. The fit values are K/μ=(3.8, 2.9, 2.1) kV/cm and N_0=(1.74, 4.51, 8.93)·10^7e and W(=E/N_0) values of (37, 44, 45) eV/e, respectively. These W values are considerably larger than the min. ion. value of 15.6 eV/e and different from the normal result observed in liquid Argon.

The fit values of K/μ imply that drift fields of (95, 72, 53) kV/cm respectively, are required to collect 98% of the charge. Improved charge collection, however, may be had by increasing the drift velocity, since ξ (in eq. 1) depends only on $v=\mu E_d$. The addition of ≈3% methane (Neopentane or TMS) is already planned to reduce pileup but it will have the added advantage of increasing the charge collection efficiency (i.e. equivalent to a factor 7 increase in field). The W values measured were stable with variation of the incident flux however the K/μ values decrease with decreasing flux indicating that the above fit values should be considered as upper limits.

These measurements point out several basic problems in liquid Xenon ionization detectors related to δ ray energies (5 to 100 keV):

1) that the W value is (≈3) times larger than for min. ion.

2) that a faster drift velocity v is needed to collect the charge.

Both of these problems may be ameliorated by simultaneous detection of scintillation light.

For δ ray energies, an increased W value may be characteristic of high density Xenon but perhaps not characteristic of lower density Krypton. Recall that an approximately normal value (W=27 eV) was seen in liquid Argon, with 66 keV electron excitation (see section 3.5.2).

3.6.2 ENERGY RESOLUTION

During this same set of runs, energy resolution from the ionization signal was measured. The variation of the incident energy was made by changing the acceleration voltage from 40 kV (≈2.6 keV electrons transmitted through the mylar window) to 95 kV (84 keV electrons transmitted) with the corresponding total energy deposit from 0.25 to 8.6 GeV. The observed energy resolution is shown in fig. 3.16 and is fit to the form $\sigma_E/E=aE^{1/2}+b$ with a=0.3% and b=1.1%. The constant term is thought to be due to as yet uncontrolled fluctuation in the electron beam flux. In several runs, under the best conditions, a high energy resolution of 0.8% was attained. This already excellent result was obtained from ionization of (2.6 to 84) keV electrons which suffer most from recombination fluctuations and high W values. It will indeed be surprising if the correlated scintillation measurement does not improve markedly upon this resolution.

4. OBJECTIVES, MILESTONES AND TIMESCALE

The long range objective of this project is to design and construct a prototype liquid Xenon calorimeter by mid 1992. The calorimeter has transverse dimensions of 10.7 X_0 and length of 28 X_0 with a sensitive volume of 71 liters and total volume of 100 liters weighing 308 kg. A refrigerator capable of condensing this quantity has been bought and tested. A mechanical and cryogenic design of the tentative calorimeter has been realized but construction awaits the completion of the laboratory measurements and the choice of the photosensor.

Proposed milestones:

1) Laboratory demonstration of excellent (≤ 1%) energy resolution from scintillation or ionization and/or from their correlation.

2) Laboratory demonstration of high efficiency detection of liquid Xenon (and Krypton) scintillation with CsI photodiodes.

3) Laboratory determination of the effect of (methane, neopentane etc.) dopants on drift velocity, scintillation yield, charge collection and W.

4) Test beam demonstration of the energy resolution attainable from scintillation in a totally active calorimeter.

5) Test beam demonstration of the direction and position resolution from ionization (and drift) in a totally active calorimeter.

5. ACTIVITIES AND RESPONSIBILITIES

5.1 CERN AND COLLEGE DE FRANCE GROUP

The mechanical and cryogenic design of the prototype calorimeter will be coordinated by this group. The construction will be the responsibility of this group. The design of the electronics and the organization of the test runs and data analysis will also be coordinated by this group.

5.2 COIMBRA GROUP

This group will set-up (at Coimbra) a cryogenic facility with an electron accelerator to study drift velocities and scintillation yields in liquid Xenon and Krypton doped with organic molecules to increase the speed of the detector without quenching the scintillation. This group will also participate in the test runs and data analysis.

5.3 PROTVINO GROUP

The responsibility for the procurement and purchase of 308 kg of Xenon. This group will also investigate the availability and price (in the USSR) of the approximately 1 ton of Krypton needed for a full prototype Krypton calorimeter. This group will participate in some of the R & D activities at CERN and take a full part in the test runs and data analysis.

6. CALORIMETER COST ESTIMATE

The schematic layout (solution 1) of the calorimeter with its cryogenic, storage and recovery systems and with a (large volume/fast recovery) storage dewar of large autonomy is shown in fig. 3.17a. A

cheaper version (solution 2) with high pressure stainless steel cylinders for Xenon gas storage supplemented by a 40 m^3 emergency recovery volume is shown in fig. 3.17b.

6.1 MECHANICAL		
Inner liquid Xenon vessel	50 kSF	
Vacuum vessel	50	
Vacuum pumps	20	
Internal calorimeter structure	40	
Cabling (feedthroghs etc.)	40	
Sub Total	200	
6.2 CRYOSYSTEM		
On line purification and cryocircuits	100	
Refrigerator	0	(already paid, 50 kSF)
Liquid Nitrogen Dewar	50	
Off-line purification	100	(use on-line, 0 kSF)
Sub Total	250	
6.3 FLUIDS		
308 kg of Xenon	0	(from IHEP, 616 kSF)
6.4 FLUID STORAGE		
Large autonomy clean dewar	200	(s.s. bottles, 50 kSF)
Compressor and batteries	30	
Sub Total	230	
6.5 CONTROLS		
Controls	50	
6.6 INSTALLATION IN BEAM	50	
6.7 ELECTRONICS		
200 Wave form digitizers	100	
100 ADC's	10	
Sub Total	110	

6.8 MANPOWER

Design	40	(0.5 man-year)
Assembly, test and installation	360	(6 man-years)
Engineering	0	(assumed part time)
Sub Total	400	
Total	890	(excluding manpower)
Total	1290	(including manpower)

7. FUNDING

7.1 FRANCE

We have requested from IN2P3 the sum of 400kFF/yr for this project divided into two elements: mechanical construction (200 kFF), electronics (200 kFF). This proposal was presented at the IN2P3 meeting at Marseille (15/10/90). No decision has yet been taken but will require (at least) a positive expression on the part of the DRDC.

7.2 PORTUGAL

A request for 100 kSF/yr was made to the JNICT ("Portugal-CERN Fund") for the construction of cryogenic facilities and an electron accelerator at Coimbra. A fellowship for a post-graduate student (67%) was also be requested.

7.3 I.H.E.P.

A commitment on the part of this laboratory to provide 200kg of Xenon has already been made. A request for the remaining 108 kg is now being considered.

7.4 CERN

A request is made for the sum of 300 kSF/yr (over a 2 year period) to partially cover the prototype construction, electronics, cleaning system and cryostat (the refrigerator has been already acquired). The outside contributions should total about 300 kSF hence the project could be on beam at the end of this two year period. This assumes that the manpower needs can be provided by CERN.

Test beam facilities will of course be needed to test the prototype calorimeters, but probably not before the year 1992. Two beams will probably be needed: a high energy (50-200 GeV/c) and a low (1-50 GeV/c) energy beam each with good dispersion for energy tagging.

Computing facilities will be limited to the 33% level as requested. The present level of computing support provided to the College de France group by IN2P3 is 400 hours CPU at CC-LYON for the first half of 1991.

Access to the CERN shops is important during the R & D phase of the project. Construction at the CERN workshops of elements of the calorimeter will be requested if suitable capabilities cannot be found at the home laboratories or commercially. The prices quoted above include workshop manpower costs.

REFERANCES

[1] The LAA Project, Liquid XENON Calorimetry, CERN-LAA/89-1, Pp 187.

[2] J.Seguinot, M.Bosteels, Y.Giomataris, A. Gougas, G.Passardi, J.Tischhauser and T.Ypsilantis. Liquid Xenon Calorimetry Progress Report (in preparation).

[3] Reflective UV photocathodes with gas phase electron extraction: Solids,liquids and adsorbed thin films. J.Seguinot, G.Charpak, Y.Giomataris, V.Peskov, J.Tischhauser and T.Ypsilantis. CERN-EP/90-88. Submitted to Nuclear Instrum. Methods A (in press).

[4] J.Seguinot, Y.Giomataris, P.Weilhammer, and T.Ypsilantis. The UV response of Silicon strip photodiodes (in preparation).

[5] J.Thomas and D.A.Imel. Phys. Rev. A36(1987)614.

[6] S.Kubota, A.Nakamoto, T.Takahashi, T.Hamada, E.Shibamura, M.Miyajima, K.Masuda and T.Doke. Physical Review B 17 (1978) 2762.

FIGURE CAPTIONS

Fig. 2.1a. A perspective view of the calorimeter cell. Its length is $2X_0$=56 mm (along the wire direction) and its transverse size is $1.07X_0$=30 mm. The readout posts, transverse walls and floor are made of carbon fiber.

Fig. 2.1b. A top view of the calorimeter tower with 14 drift cells, transverse reflective walls and the photosensor (hatched) at the far end.

Fig. 2.2. A perspective view of the prototype calorimeter with its towers, readout columns and the collection wire planes (and electroformed Frisch grids).

Fig. 2.3a. The ionization and trigger signals (versus time) generated in a single tower by a 25 GeV photon at t=0 followed by a 50 GeV photon at t=550 ns.

Fig. 2.3b. The scintillation signals (versus time) generated by the above events. Note that these signals are coincident with (and part of) the trigger signals and they amplitude tag the time origin of the ionization signals which are otherwise ambiguous.

Fig. 2.4. A plan view of the calorimeter cells (and towers) with the projected energy deposit due to a 1 GeV electron incident from the left.

Fig. 2.5a. The energy deposit in the first depth cell (E_1) versus transverse coordinates (x_1, y_1) with binning $\Delta x=\Delta y=0.5$ mm from a 1 GeV electron.

Fig. 2.5b. The energy deposit in the second depth cell (E_2) versus transverse coordinates (x_2, y_2) with binning $\Delta x=\Delta y=0.5$ mm from a 1 GeV electron.

Fig. 2.6a. The angular resolution σ_θ versus the number of depth cells used in the straight line fit for 10, 25 GeV electrons. The cuts signify that only energy deposits with more than (10, 20, or 30%) of the peak are used (i.e. tail suppression).

Fig. 2.6b. The vertex position resolution (normal projection) σ_p versus the number of depth cells used in the straight line fit for 10, 25 GeV

electrons. The cuts signify that only energy deposits with more than (10, 20, or 30%) of the peak are used (i.e. tail suppression).

Fig. 3.1 The measured detected quantum efficiency Q (photoelectrons per incident photon) versus photon wave length λ for a Silicon microstrip photodiode (DELPHI) and for a reflective CsI thin film.

Fig. 3.2 A side view of the 100 kV electron accelerator with the UV flash lamp, accelerating structure and the liquid Xenon test cell.

Fig. 3.3 The cryostat, condenser and filtering system used to purify noble liquids.

Fig. 3.4 The obseved ionization signal N_{pe} versus circulation time through the filters. The closed points correspond to the initial Xenon which was badly contaminated while the open points are for precleaned Xenon. The asymptotic lifetimes attained were 4 and 100 μs, respectively.

Fig. 3.5 The arrangement of the test cell used to observe scintillation from liquid and gaseous Xenon. The scintillation signal was observed with a CsTe solar blind PM with a MgF_2 window. The liquid level was varied to determine its transparency.

Fig. 3.6a. The observed liquid Xenon scintillation wave form. After the quadrature subtraction of the lamp signal the lifetime $\tau \approx 13$ ns.

Fig. 3.6b. The observed gaseous Xenon (1 bar) scintillation wave form with a long recombination tail ($\tau \approx 60$ ns).

Fig. 3.7. The observed liquid Xenon scintillation signal (photons/MeV) versus the liquid level height h. No apparent absorption was seen in traversing 2 cm of liquid Xenon path length.

Fig.3.8a. The liquid Xenon scintillation signal (N_{pe} photoelectrons) versus the E (total energy/pulse) deposited in the test cell.

Fig.3.8b. The fractional variance of the liquid Xenon scintillation signal (σ_E/E) versus E the (total energy/pulse) deposited in the test cell. The

open points are the data and the closed points are the contribution to the resolution from photoelectron statistics $1/\sqrt{N_{pe}}$.

Fig. 3.9 The arrangement of the test cell for simultaneous observation of ionization and scintillation. The ionization signal is collected on the anode mesh and the scintillation signal is observed as a current in the Silicon strip photodiode. The Faraday-cage collimator which monitors rhe incident charge is indicated.

Fig. 3.10a. The ionization signal (I) collected versus the drift field (E_d).

Fig. 3.10b. The scintillation signal (S) collected versus the drift field (E_d).

Fig. 3.10c. A scatter plot of ionization signal (I) versus the scintillation signal (S) for a fixed field E_d and energy deposit E (as determined by the Faraday-cage collimator).

Fig. 3.11a. The linearity of the ionization signal (I) versus energy (E).

Fig. 3.11b. The linearity of the scintillation signal (S) versus energy (E).

Fig. 3.12a. The ionization signal (I) in liquid Argon versus the drift field (E_d) with a fit of the single charge-density model (eq. 1).

Fig. 3.12b. The scintillation signal ($S=N_{pe}$) in liquid Argon versus the drift field (E_d) with the above curve transcribed from the condition $I+\alpha S=\beta$. Note that the transcribed curve well fits this data considering that only two points were used to determine (α, β).

Fig. 3.13. The energy resolution (σ_E/E) from ionization in liquid Argon versus E the (total energy/pulse) deposited in the test cell.

Fig. 3.14. The waveform of the collected charge versus drift time when the electron lifetime in liquid Xenon was long ($\tau \geq 100$ μs). The slight curvature is due to the electronic respose time ($t_e=26.7$ μs).

Fig. 3.15. The ionization signal ($I=N_e$) versus drift field E_d for deposited total energies of E=0.64, 1.97 and 4.02 GeV. The fit curves are from the single charge-density model (eq. 1). Interpretation of these excellent fits is given in the text.

Fig. 3.16. The energy resolution (σ_E/E) from ionization in liquid Xenon versus E the (total energy/pulse) deposited in the test cell.

Fig. 3.17a. A schematic layout (solution 1) of the calorimeter with its cryogenic, storage and recovery systems with a (large volume/fast recovery) storage dewar of large autonomy.

Fig. 3.17b. A cheaper version (solution 2) with high pressure stainless steel cylinders for Xenon gas storage supplemented by a 40 m^3 emergency recovery volume.

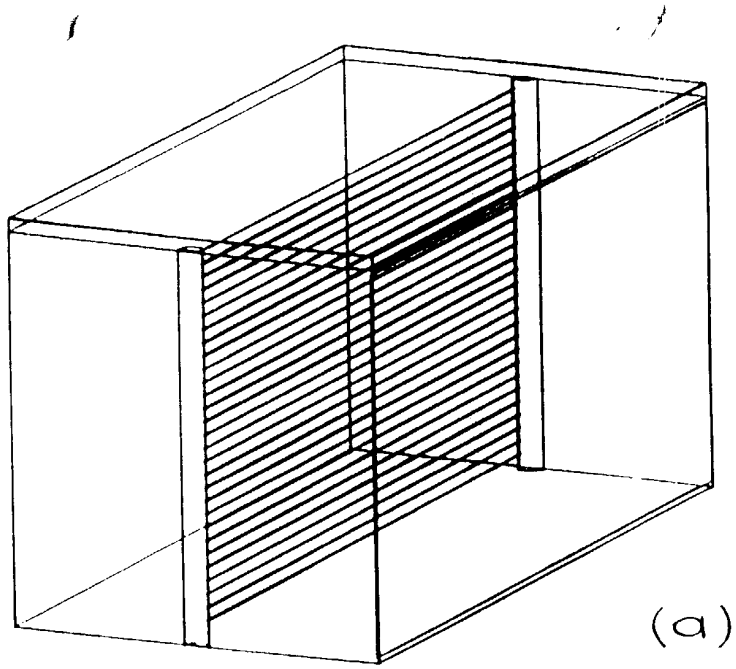

(b)

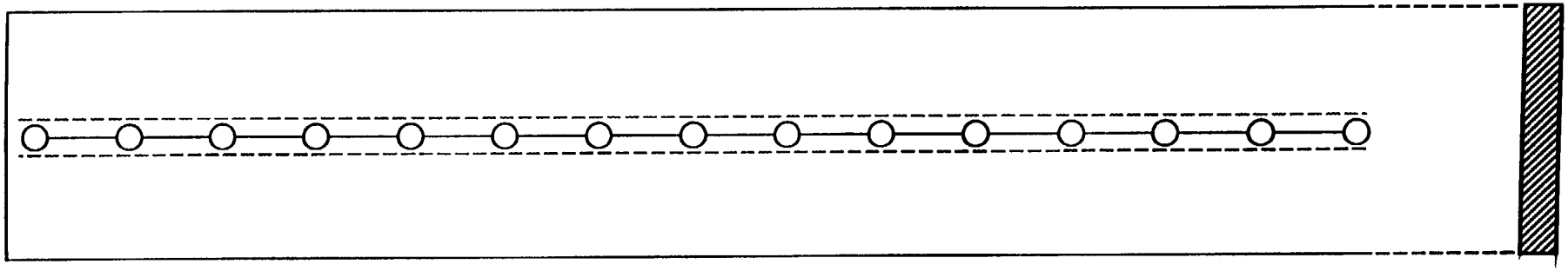

Fig 2.1

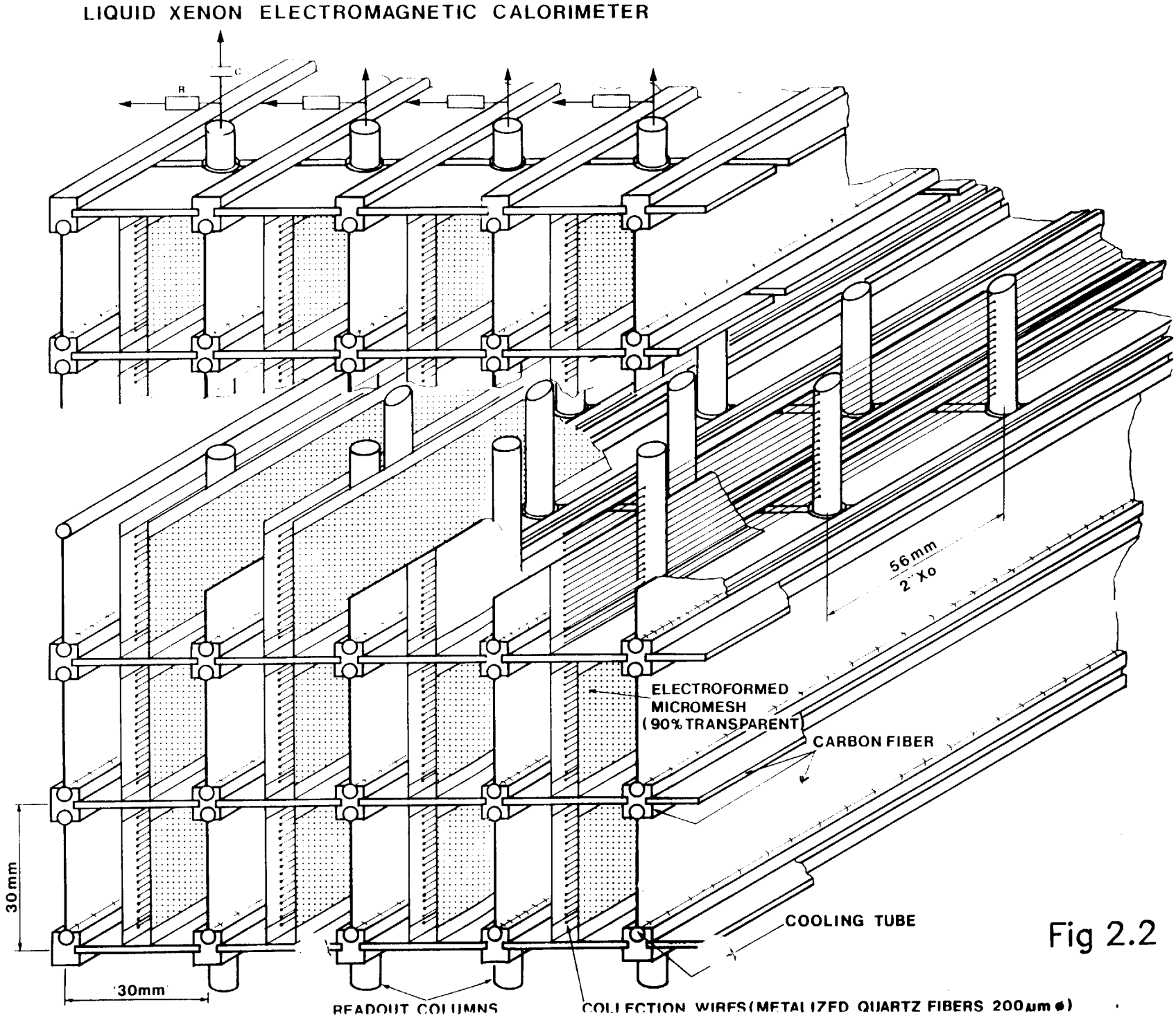
LIQUID XENON ELECTROMAGNETIC CALORIMETER
C
R
56mm
2 Xo
ELECTROFORMED
MICROMESH
(90% TRANSPARENT)
CARBON FIBER
30mm
30mm
COOLING TUBE
READOUT COLUMNS
COLLECTION WIRES (METALIZED QUARTZ FIBERS 200μm ϕ)

Fig 2.2

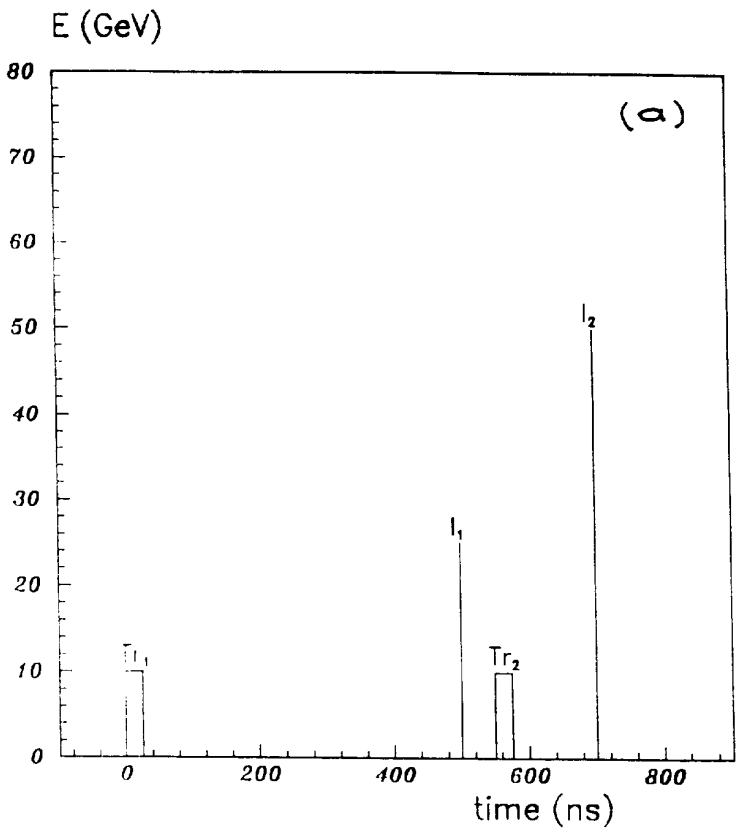
E (GeV)
(a)
80
70
60
50
40
30
20
10
0
0
200
400
600
800
time (ns)
I_1
I_2
Tr_2

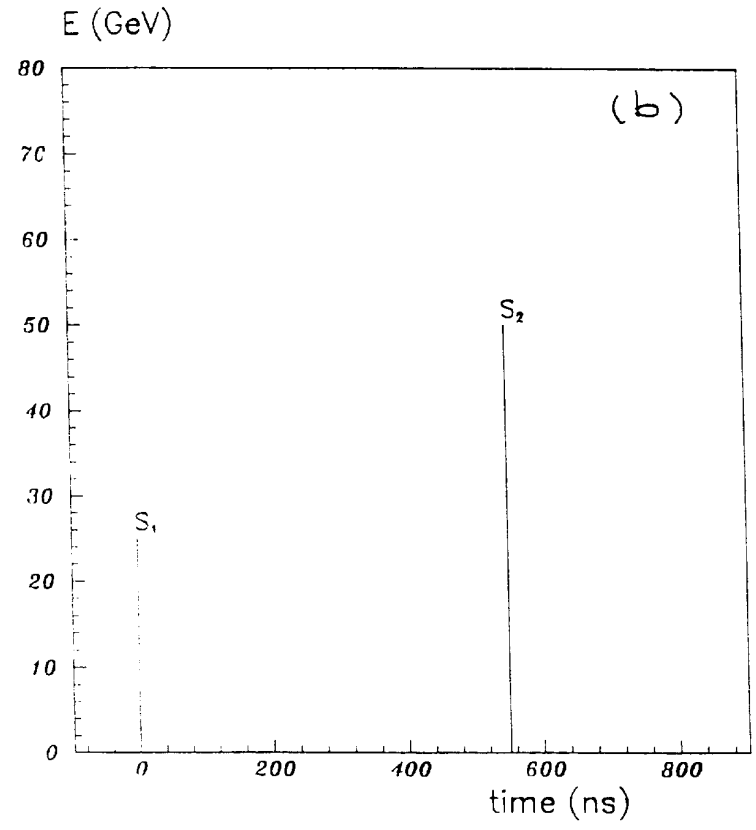
E (GeV)
(b)
80
70
60
50
40
30
20
10
0
0
200
400
600
800
time (ns)
S_1
S_2

Fig 2.3

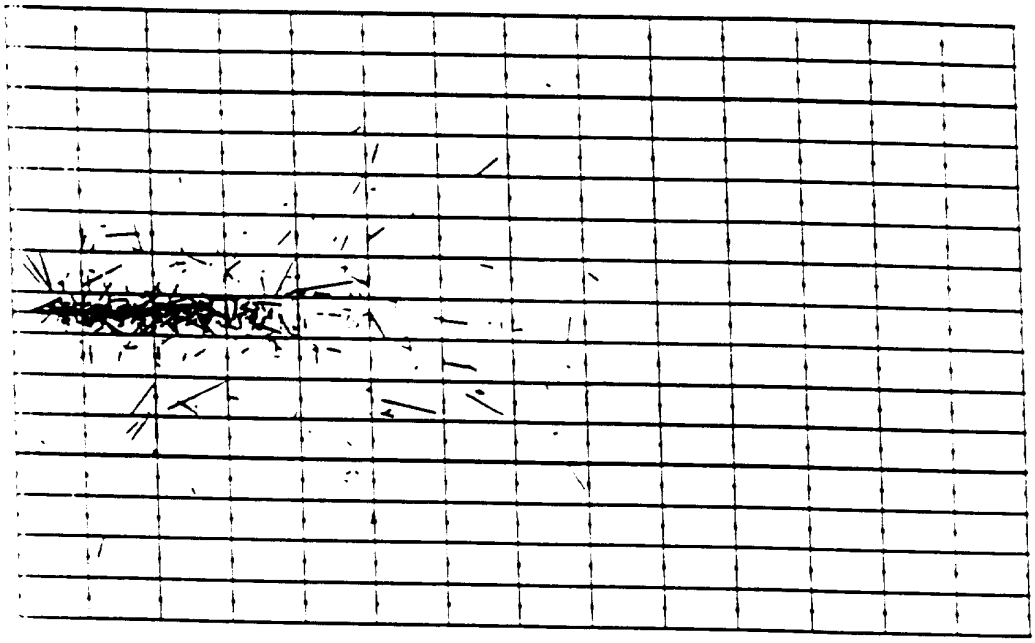

Fig 2.4

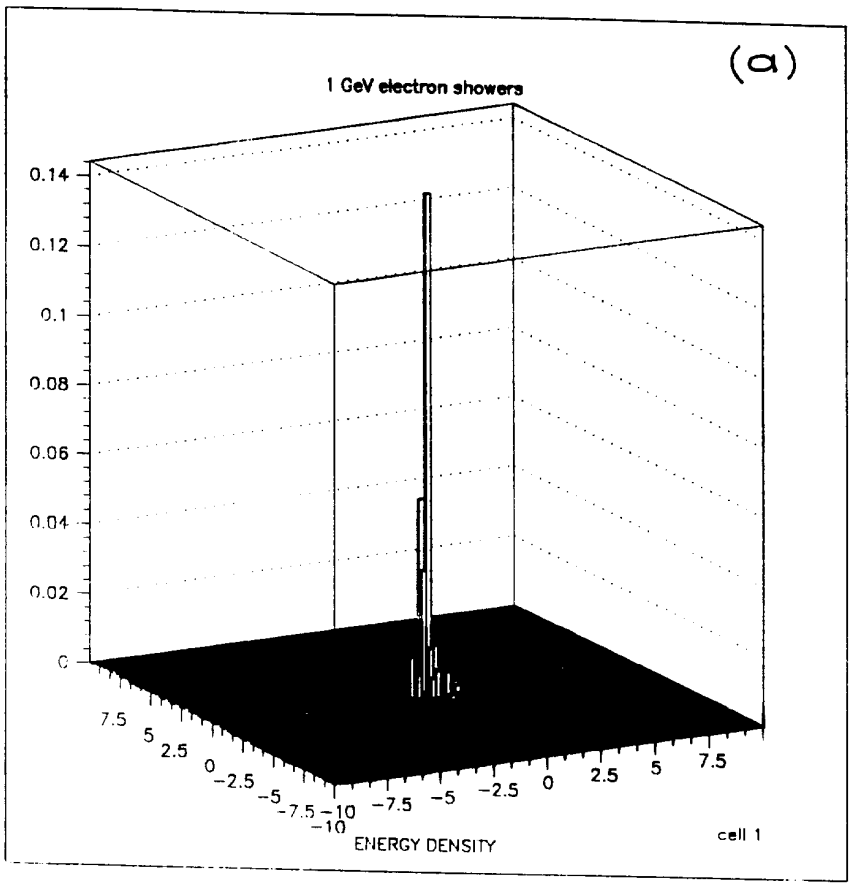
(a)
1 GeV electron showers
0.14
0.12
0.1
0.08
0.06
0.04
0.02
0
7.5
5
2.5
0
-2.5
-5
-7.5
-10
-10
-7.5
-5
-2.5
0
2.5
5
7.5
ENERGY DENSITY
cell 1

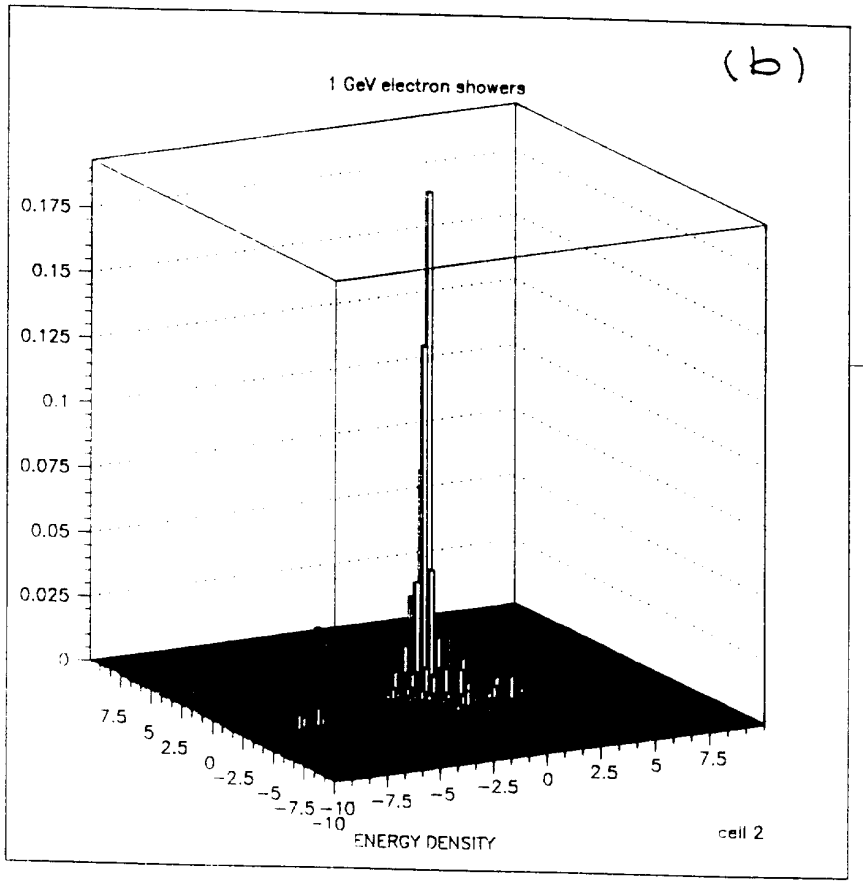
(b)
1 GeV electron showers
0.175
0.15
0.125
0.1
0.075
0.05
0.025
0
7.5
5
2.5
0
-2.5
-5
-7.5
-10
-10
-7.5
-5
-2.5
0
2.5
5
7.5
ENERGY DENSITY
cell 2

Fig 2.5

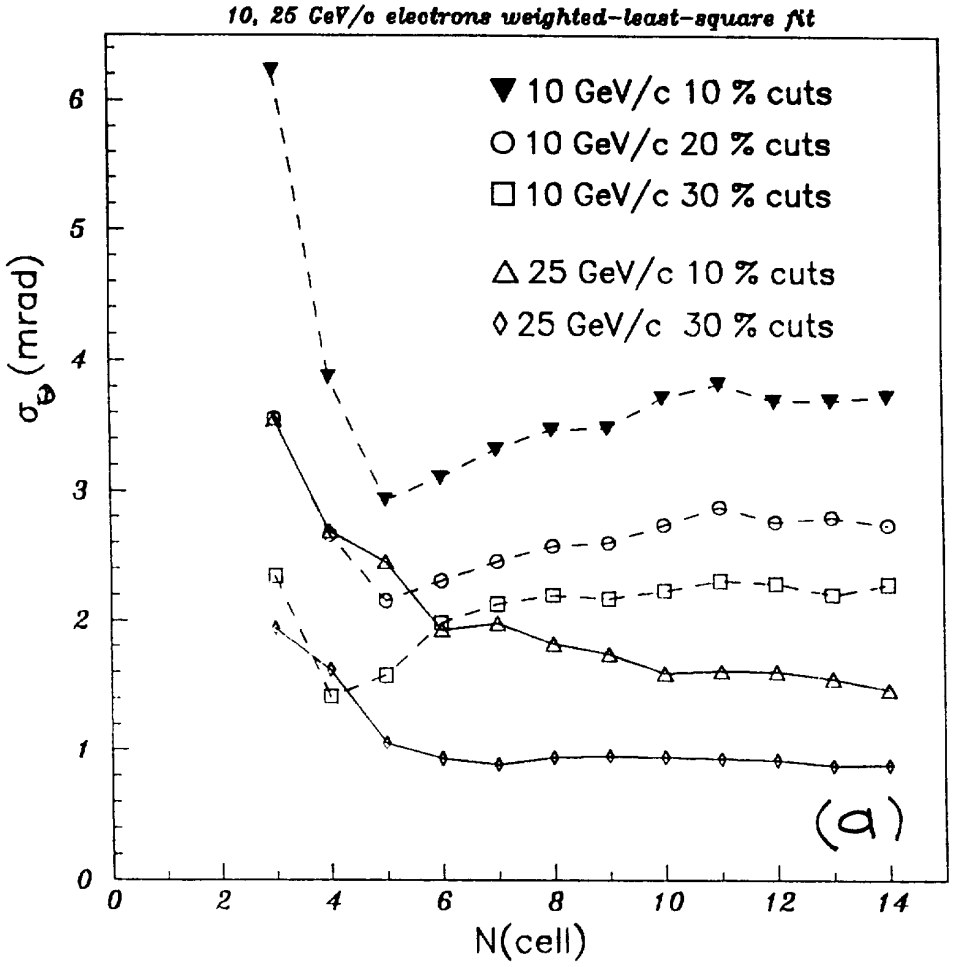
10, 25 GeV/c electrons weighted-least-square fit
▼ 10 GeV/c 10 % cuts
○ 10 GeV/c 20 % cuts
□ 10 GeV/c 30 % cuts
△ 25 GeV/c 10 % cuts
◊ 25 GeV/c 30 % cuts
σ_Φ (mrad)
N(cell)
(a)

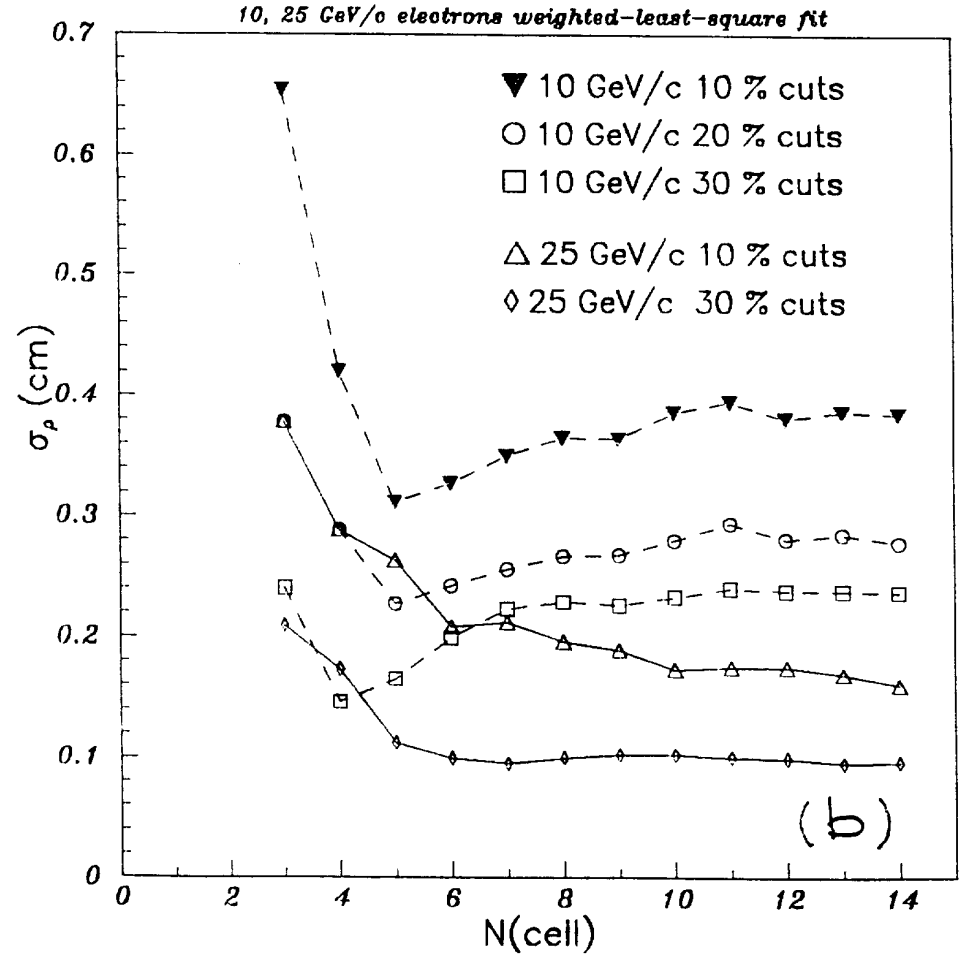
10, 25 GeV/c electrons weighted-least-square fit
▼ 10 GeV/c 10 % cuts
○ 10 GeV/c 20 % cuts
□ 10 GeV/c 30 % cuts
△ 25 GeV/c 10 % cuts
◊ 25 GeV/c 30 % cuts
σ_ρ (cm)
N(cell)
(b)

Fig 2.6

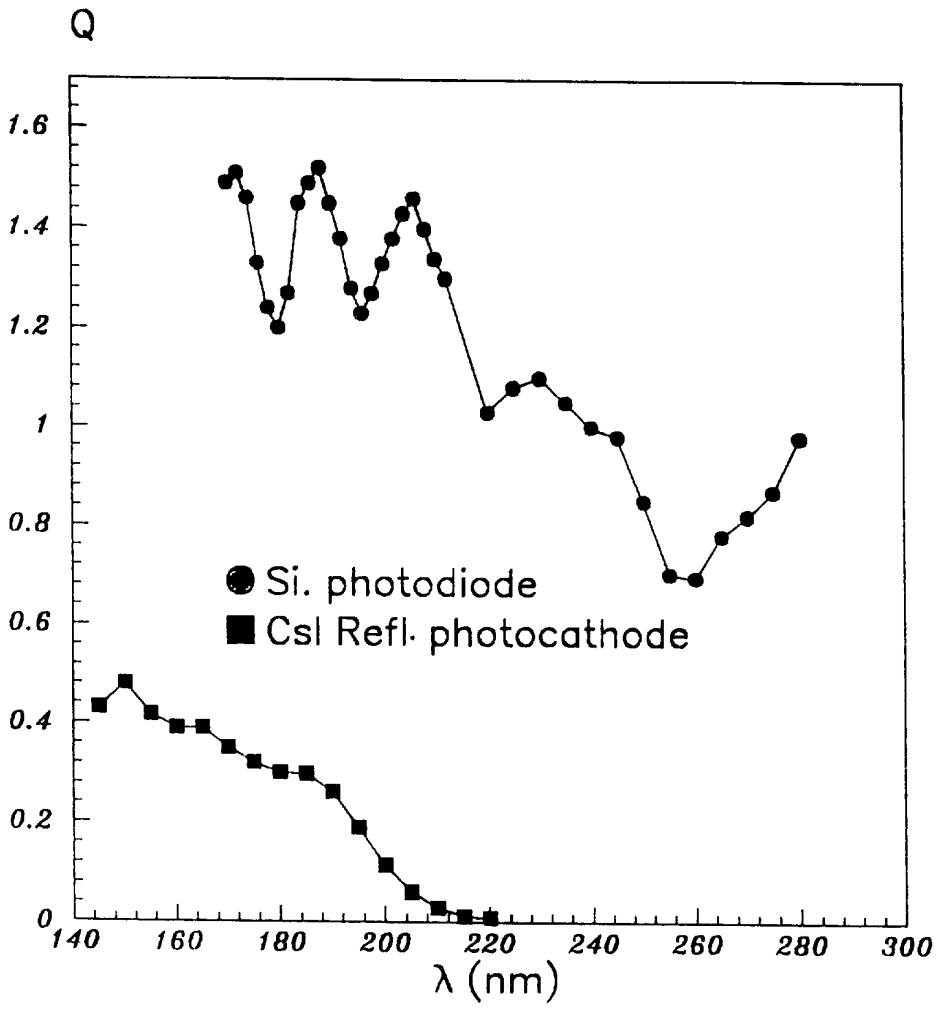
Q
1.6
1.4
1.2
1
0.8
0.6
0.4
0.2
0
140
160
180
200
220
240
260
280
300
λ (nm)
Si. photodiode
CsI Refl. photocathode

Fig 3.1

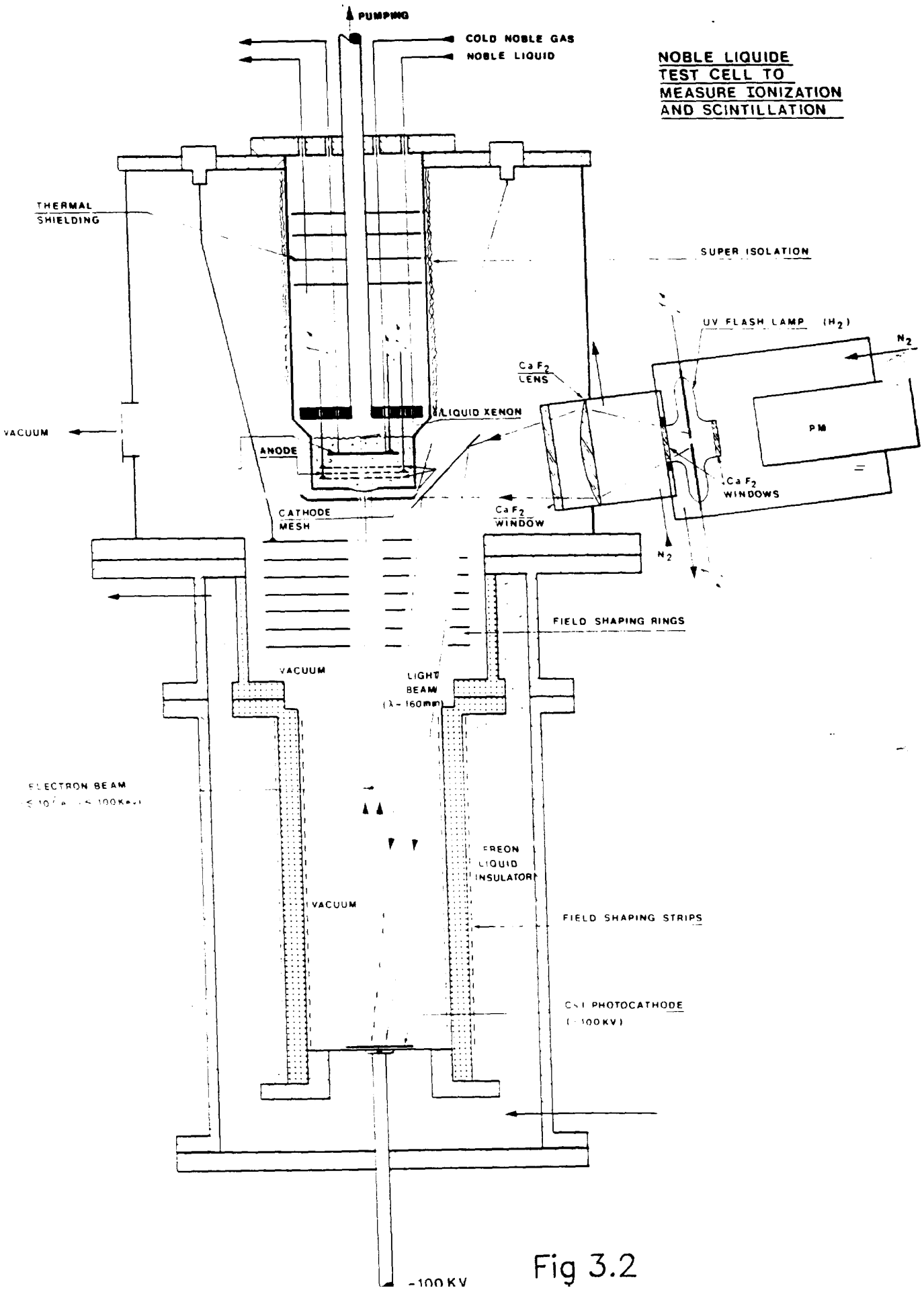
PUMPING
COLD NOBLE GAS
NOBLE LIQUID
NOBLE LIQUIDE TEST CELL TO MEASURE IONIZATION AND SCINTILLATION
THERMAL SHIELDING
SUPER ISOLATION
UV FLASH LAMP (H2)
N2
CaF2 LENS
LIQUID XENON
VACUUM
ANODE
PM
CaF2 WINDOWS
CATHODE MESH
CaF2 WINDOW
N2
FIELD SHAPING RINGS
VACUUM
LIGHT BEAM (λ ~ 160mμ)
ELECTRON BEAM
FREON LIQUID INSULATOR
VACUUM
FIELD SHAPING STRIPS
CsI PHOTOCATHODE
(-100KV)
-100 KV

Fig 3.2

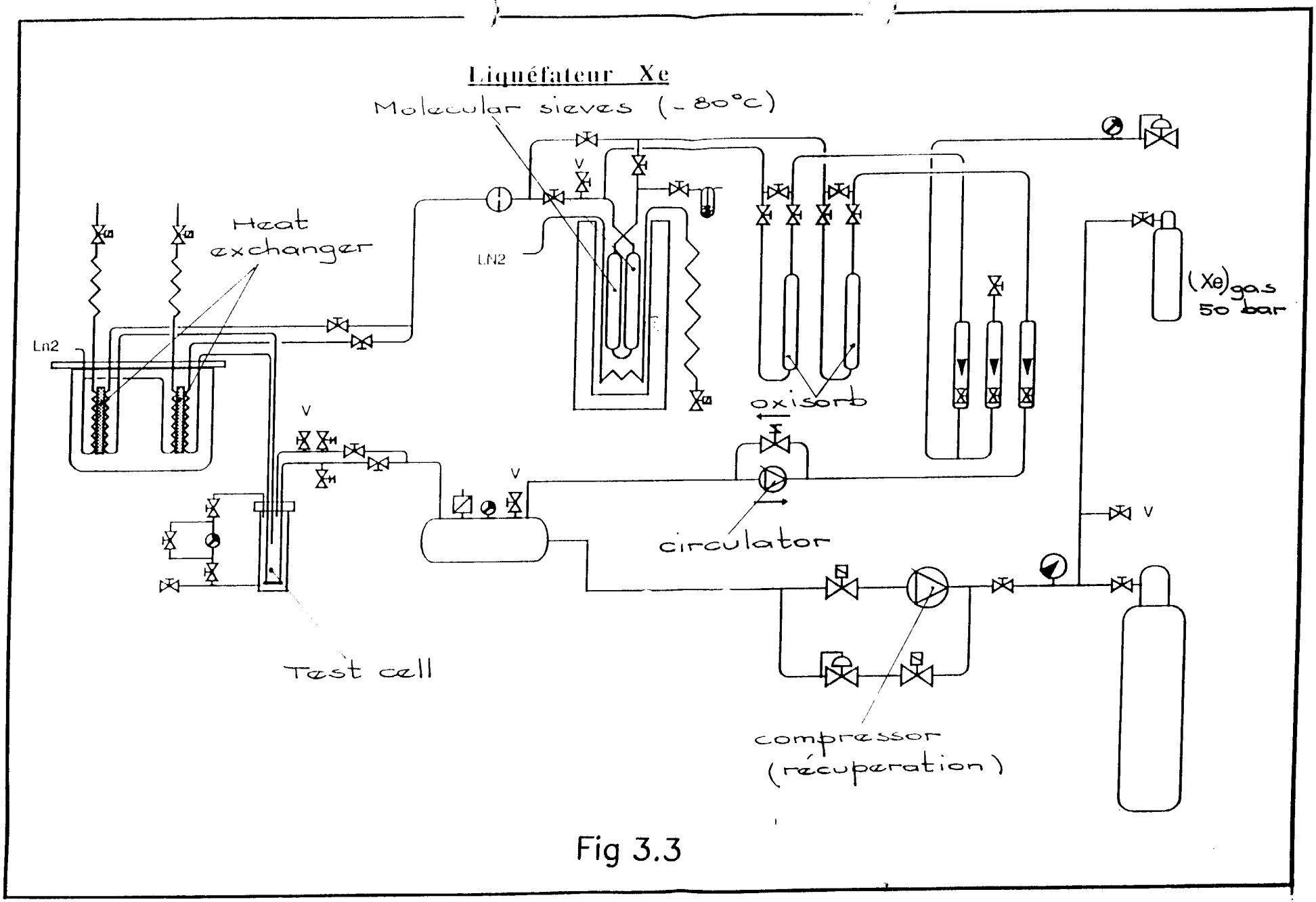
Liquéfateur Xe
Molecular sieves (-80°C)
Heat exchanger
LN2
LN2
V
V
V
V
oxisorb
circulator
(Xe) gas 50 bar
Test cell
compressor (récuperation)

Fig 3.3

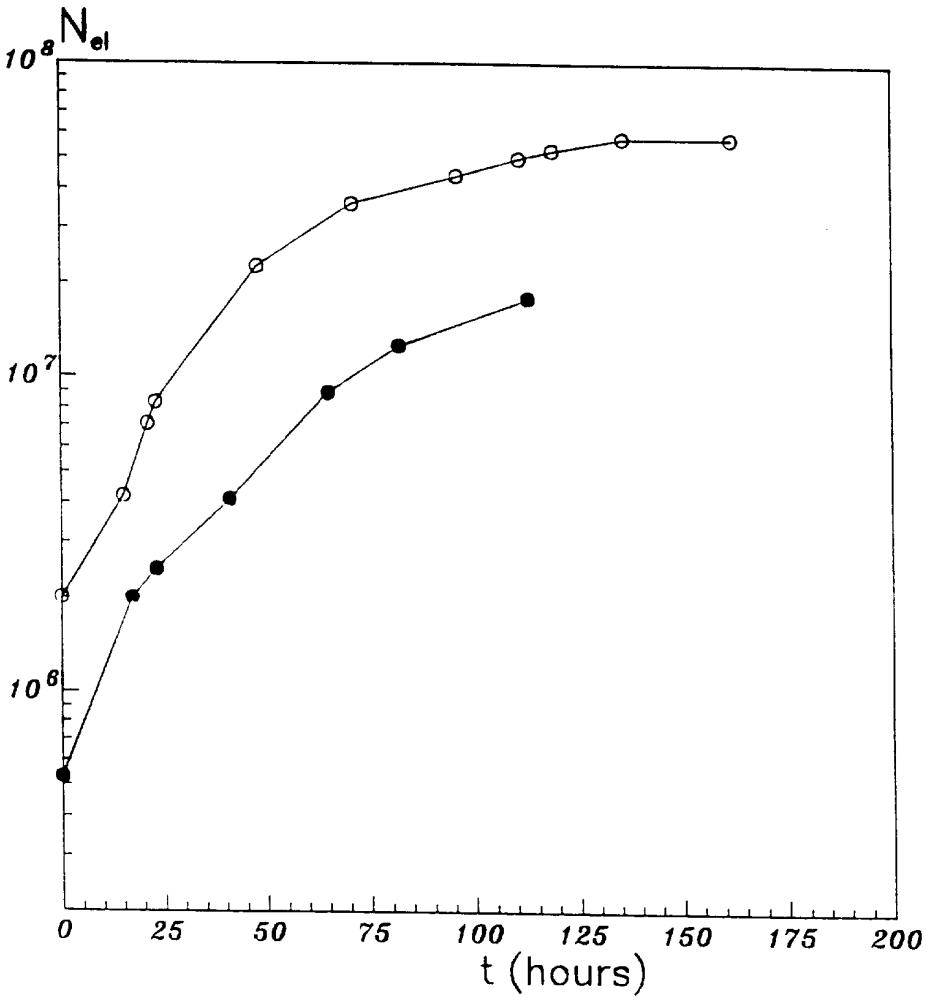

Fig 3.4

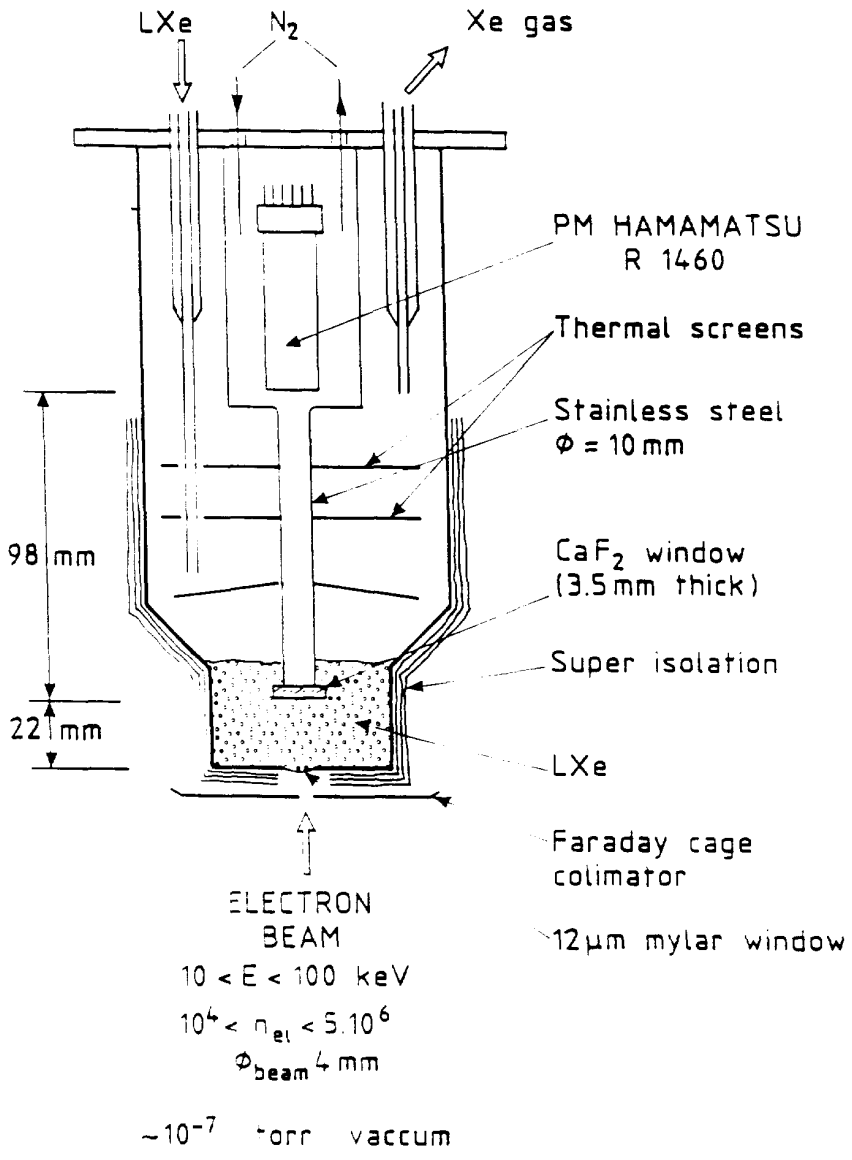
LXe
N_2
Xe gas
PM HAMAMATSU
R 1460
Thermal screens
Stainless steel
Φ = 10 mm
98 mm
CaF_2 window
(3.5 mm thick)
Super isolation
22 mm
LXe
Faraday cage
colimator
12 μm mylar window
ELECTRON
BEAM
10 < E < 100 keV
$10^4 < n_{el} < 5.10^6$
Φ_{beam} 4 mm
$\sim 10^{-7}$ torr vaccum

Fig 3.5

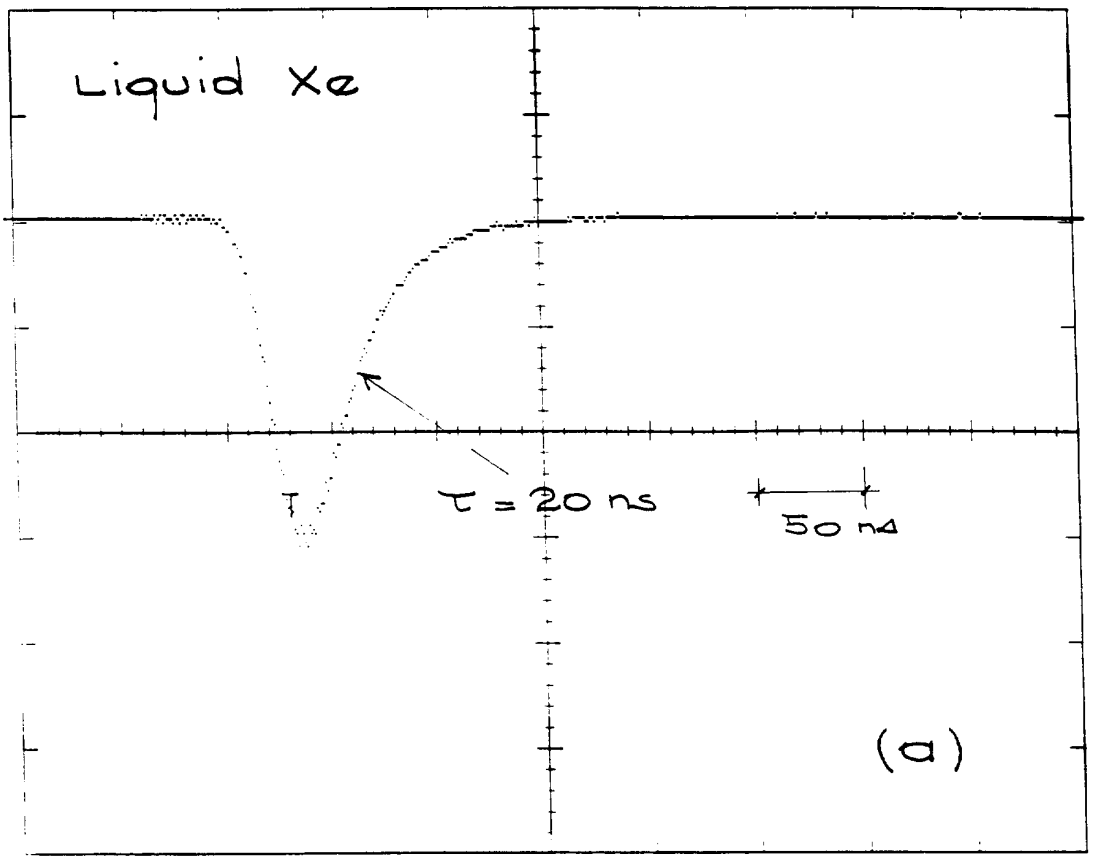

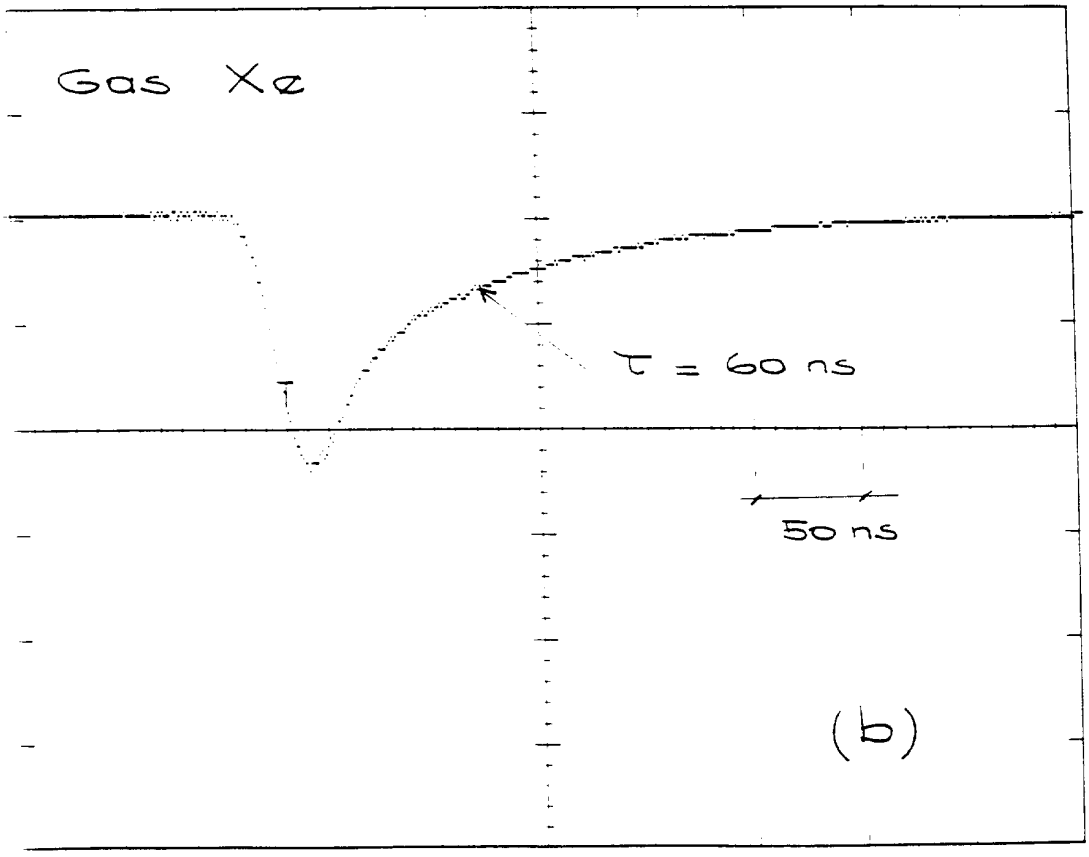

Fig 3.6

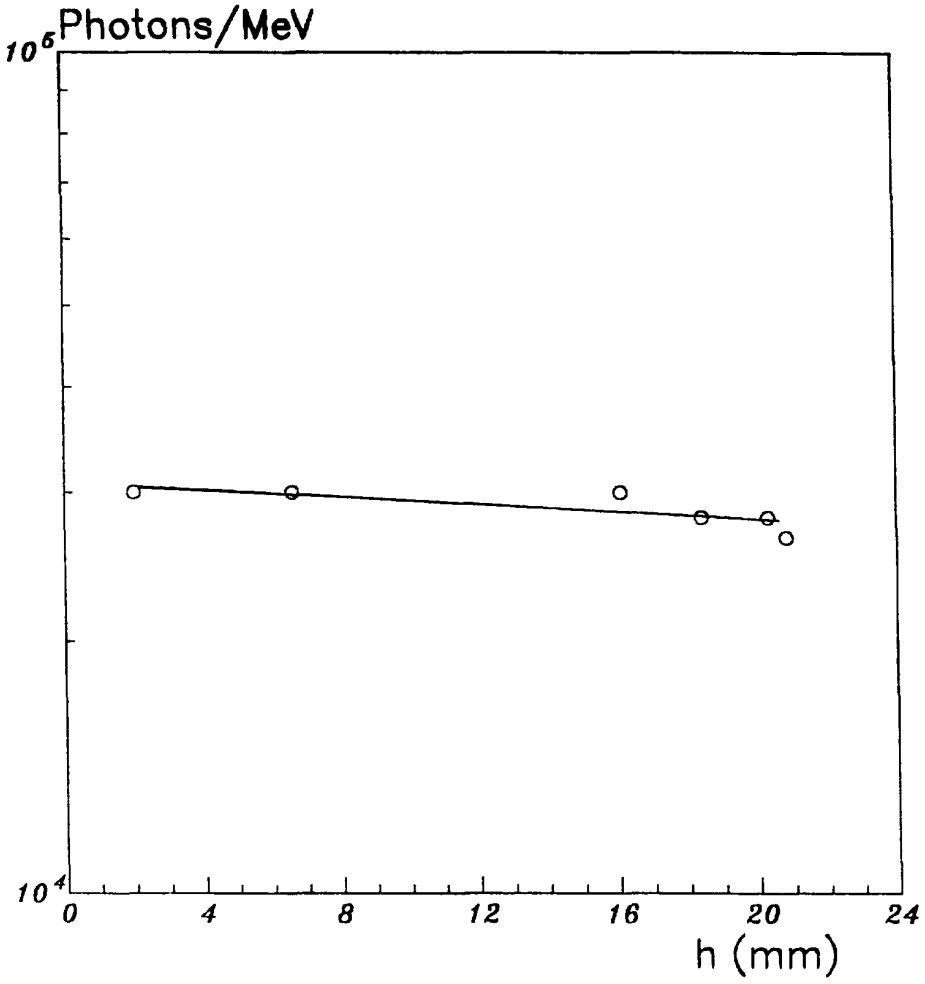

Fig 3.7

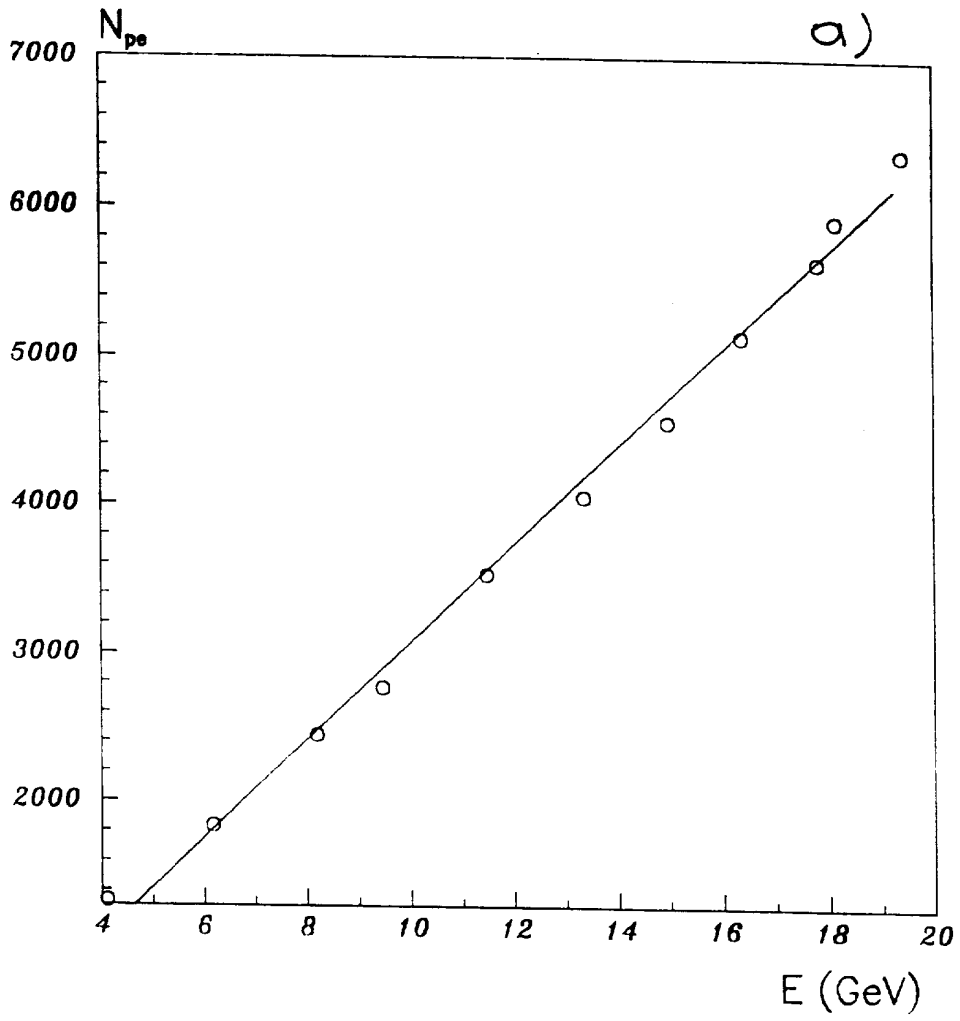
a)
N_{pe}
7000
6000
5000
4000
3000
2000
4
6
8
10
12
14
16
18
20
E (GeV)

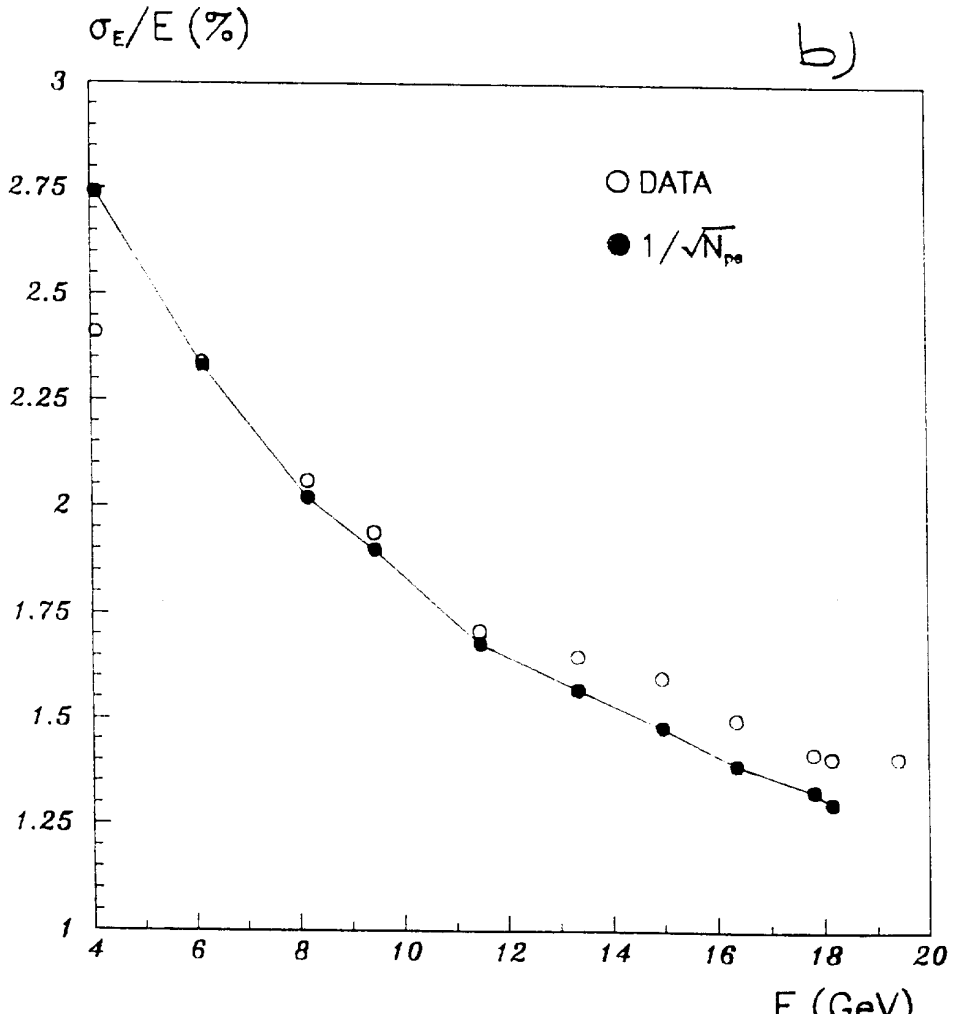
b)
σ_E/E (%)
3
2.75
2.5
2.25
2
1.75
1.5
1.25
1
O DATA
● $1/\sqrt{N_{pe}}$
4
6
8
10
12
14
16
18
20
E (GeV)

Fig 3.8